Differences in surface chemistry of regenerated lignocellulose fibers determined by chemically sensitive scanning probe microscopy

International Journal of Biological Macromolecules 165 (2020) xxx

Contents lists available at ScienceDirect

International Journal of Biological Macromolecules

journal homepage: http://www.elsevier.com/locate/ijbiomac

Differences in surface chemistry of regenerated lignocellulose fibers determined by chemically sensitive scanning probe microscopy

Claudia Gusenbauer [a,*], Tiina Nypelö [b,c], Devon S. Jakob [d], Xiaoji G. Xu [d], Dmitri V. Vezenov [d], Shirin Asaadi [e], Herbert Sixta [e], Johannes Konnerth [a]

[a] Institute of Wood Technology and Renewable Materials, Department of Materials Sciences and Process Engineering, BOKU-University of Natural Resources and Life Sciences Vienna, Konrad-Lorenz-Straße 24, 3430 Tulln, Austria
[b] Applied Chemistry, Department of Chemistry and Chemical Engineering, Chalmers University of Technology, 41296 Gothenburg, Sweden
[c] Wallenberg Wood Science Center (WWSC), Chalmers, Gothenburg, Sweden
[d] Department of Chemistry, Lehigh University, 6 East Packer Avenue, Bethlehem, PA 18015, USA
[e] Department of Bioproducts and Biosystems, Aalto University, P.O. Box 16300, 00076 Aalto, Finland

ARTICLE INFO

Article history:
Received 27 August 2020
Received in revised form 25 September 2020
Accepted 17 October 2020
Available online 23 October 2020

Keywords:
Atomic force microscopy
Ioncell-F
Lignocellulose

ABSTRACT

Tuning the composition of regenerated lignocellulosic fibers in the production process enables targeting of specific material properties. In composite materials, such properties could be manipulated by controlled heterogeneous distribution of chemical components of regenerated fibers. This attribute requires a visualization method to show their inherent chemical characteristics. We compared complementary microscopic techniques to analyze the surface chemistry of four differently tuned regenerated lignocellulosic fibers. Adhesion properties were visualized with chemical force microscopy and showed contrasts towards hydrophilic and hydrophobic atomic force microscopy tips. Fibers containing xylan showed heterogeneous adhesion properties within the fiber structure towards hydrophilic tips. Additionally, peak force infrared microscopy mapped spectroscopic contrasts with nanometer resolution and provided point infrared spectra, which were consistent to classical infrared microscopy data. With this setup, infrared signals with a spatial resolution below 20 nm reveal chemical gradients in specific fiber types.

1. Introduction

The Ioncell-F process of the Lyocell type provides a recently developed group of regenerated fibers that contribute towards a more sustainable and biobased textile industry [1]. The derived man-made cellulosic materials stand out in terms of their chemical stability and high elastic moduli [2]. These characteristics are superior to those of e.g. viscose fibers and originate from dissolving and spinning cellulosic resources in ionic liquids at mild temperatures, resulting in less degraded and highly oriented cellulose structures compared to viscose fibers [3]. Alongside improved structural and mechanical features, lower energy and solvent consumption in the fabrication benefit the Ioncell-F process [4].

Besides the textiles, natural fibers can be found in cellulosic fiber-reinforced polymeric composites. For instance, natural fibers are used in the automotive industry due to their high specific strength and high abundance in plant materials [5]. One type of a composite material made solely of renewable resources is formed by embedding regenerated fibers of the Lyocell type in a polylactic acid (PLA) matrix and shows improved Young's moduli, tensile and impact strength [6,7]. The challenge in manufacturing such “green” composites arises from the incompatibility between the hydrophilic nature of natural fiber materials and the more hydrophobic polymeric matrix. To overcome this limitation, lignin obtained from eucalyptus trees was identified as a natural additive to improve the compatibility and interfacial shear strength [8]. Additionally, hemicellulose (xylan) from beech wood influences the fiber morphology, i.e., altered fiber cross sections and frictional properties [9]. Based on the beneficial attributes of these two natural additives, which imitate the composition of wood fibers together with cellulose, the surface properties of the regenerated fibers, such as polarity, can be regulated by adjusting the amount of the three components - cellulose, lignin, and xylan - in Ioncell-F fibers. Atomic force microscopy (AFM) in air showed that lignin decreased adhesion forces towards standard silicon tips, while xylan increased the adhesion forces [10]. Raman microscopy measurements could not be conducted due to the

* Corresponding author at: University of Natural Resources and Life Sciences, Vienna, Department of Material Sciences and Process Engineering (MAP), Institute of Wood Technology and Renewable Materials, Konrad Lorenz Straße 24, 3430 Tulln, Austria.
E-mail addresses: claudia.gusenbauer@boku.ac.at (C. Gusenbauer), tiina.nypelo@chalmers.se (T. Nypelö), dsj316@lehigh.edu (D.S. Jakob), xgx214@lehigh.edu (X.G. Xu), dvezenov@lehigh.edu (D.V. Vezenov), shirin.asaadi@alumni.aalto.fi (S. Asaadi), herbert.sixta@aalto.fi (H. Sixta), johannes.konnerth@boku.ac.at (J. Konnerth).

https://doi.org/10.1016/j.ijbiomac.2020.10.145
0141-8130/

auto-fluorescence of the lignocellulosic fibers. In another study, adhesion forces were studied by a colloidal probe technique in air or dry nitrogen atmosphere, in which adhesion properties between PLA microspheres and regenerated lignocellulosic fibers were examined. It was revealed that lignin and xylan increase adhesion forces, suggesting their beneficial impact on the improvement of the compatibility with PLA [11].

It has been suggested that the optimized regenerated fibers display an inhomogeneous distribution of chemical components and favor a skin-core structure [12–14] that affects the interface between components of the composite materials. Specifically, the enrichment of the surface/skin region with the hemicellulose would enhance the affinity between the fibers and the matrix materials. The previous adhesion studies were performed in either air or nitrogen environment and, therefore, were highly influenced by capillary forces and had limitations in the localization of functional groups. On the other hand, in-depth structural and mechanical studies of the Ioncell-F fiber analyzed the crystalline/amorphous domains and the influence of voids [2] but lacked complementary information on the chemical characteristics of the fiber structure. Therefore, proper analysis tools are required to address whether enrichment phenomena of chemical components occur in fibers obtained by the Ioncell-F process.

Here, we focus on AFM-based techniques to visualize surface chemical variances at cross-sections of specifically tuned Ioncell-F fibers embedded in a PLA matrix. Chemical force microscopy (CFM) has been identified as a powerful AFM technique to monitor the distribution of functional groups by scanning the surfaces of cellulosic fibers with distinct chemically modified tips under liquids [15–17]. In this paper, we hypothesize that the cross-section of Ioncell-F fibers shows a heterogeneous distribution of chemical surface characteristics. Since CFM was able to map heterogeneous distribution of adhesion forces on lignocellulosic surfaces [18,19], we performed CFM measurements with – OH and – CH_3 functionalized AFM tips in liquid media to trace the surface chemical properties of Ioncell-F fibers with high spatial resolution. The analysis of adhesion forces shall reveal the extent of the compatibility between the lignocellulosic fibers and PLA matrix. Complementary, we applied peak force infrared microscopy (PFIR) measurements as a novel AFM tool being able to gain simultaneously chemical and mechanical contrasts with <10 nm resolution [20–22]. By focusing a pulsed infrared laser between the tip apex and the surface of the sample, variation in the thermal expansion can be interpreted as infrared absorption to visualize the surface chemical behavior.

2. Experimental

2.1. Preparation of lignocellulosic fibers

Regenerated cellulose fibers were obtained from an Ioncell-F process. A detailed description of the fiber production can be found in previous publications [3,10]. Ioncell-F fibers were drawn from four different kinds of dopes dissolved in an ionic liquid (1,5-diazabicyclo [4.3.0]non-5-enium acetate; [DBNH]OAc) with a targeted amount of cellulose (from Enocell birch prehydrolysis kraft pulp, Stora Enso, Finland), xylan (from birch kraft pulp) and/or lignin (from beechwood organosolv lignin, Fraunhofer Institute CBP, Germany) within one fiber type. The dopes were spun at different take-up velocities and therefore with different draw ratios, resulting in various diameters allowing us to distinguish between the fibers in the course of characterization.

The chemical composition was determined in previous research by the NREL standard/TP510–42618 17 [10], which revealed the composition of the regenerated cellulose fibers. Fiber type one referred to as "cellulose-lignin", was spun at a draw ratio (DR) of 0.5 and is composed of 71.3 wt% cellulose, 24.3 wt% lignin, and 4.4 wt% xylan. Fiber type two, referred to as "cellulose-lignin-xylan" (DR = 7), consists of 52.8% cellulose, 23.7 wt% xylan, and 22.9 wt% lignin. Fiber type three, referred to as "cellulose" (DR = 0.5), comprises mainly cellulose (94.2 wt%) and residual xylan (5.5 wt%). Fiber type four, referred to as "cellulose-xylan" (DR = 7), is made up of 78.2 wt% cellulose, 19.6 wt% xylan, and 2.3 wt % lignin.

2.2. ATR-FTIR spectroscopy

FTIR (Fourier-transform infrared) spectra were acquired from the regenerated cellulose fibers with an attenuated total reflectance Fourier transform infrared spectroscope (ATR-FTIR, Perkin Elmer Frontier, Waltham, MA, USA). Three spectra were acquired per fiber type. The resolution was set to 2 cm^{-1}, ranging from 1768 to 900 cm^{-1} performed by four scans. The spectra were averaged, baseline corrected and normalized at 1026 cm^{-1} with a spectroscopy software (Spectragryph 1.2, Oberstdorf, Germany); the results were visualized with OriginPro 2016 (OriginLab, Northampton, MA, USA).

2.3. Embedding and surface preparation

Polylactic acid (PLA) was purchased from Natureworks (Ingeo™ 3052D, Minnetonka, MN, USA) with a D-lactide content of 4%. Four fibers (one per regenerated fiber composition) were embedded in PLA, which provided stability to scan their cross-section [11]. Therefore, PLA was heated up to 250 °C, and the fibers were closely and carefully aligned in molten PLA (Fig. 1). Thereafter, small cubes (4 mm^3) were cut out of the hardened blocks with razor blades and glued onto metal discs. The cross-sections of the fibers were subsequently cut via an ultramicrotome (Ultracut-R, Leica, Wetzlar, Germany) with diamond knives (DiATOME, Nidau, Switzerland) to generate smooth surfaces.

2.4. Chemical force microscopy

Chemical force microscopy (CFM) measurements were performed with an atomic force microscope (AFM, Dimension Icon scanning probe microscope with Nanoscope *V* controller, Bruker, Santa Barbara, CA, USA). Chemically modified tips were purchased with two different functionalities. CH_3-terminated tips (ST-PNP-CH3, nominal spring constant = 0.32 N/m, resonance frequency = 67 kHz, SmartTip, Enschede, Netherlands) or OH-terminated tips (ST-PNP-OH, nominal spring constant = 0.32 N/m, resonance frequency = 67 kHz, SmartTip, Enschede, Netherlands) were cleaned with ethanol, dried with nitrogen and put onto the AFM scan head. The ultra-microtomed lignocellulosic surfaces were placed on a fluid cell at the AFM scanning stage. For measurements performed with CH_3-tips, the fluid cell was filled with water (MilliQ, 18 MΩ, Labexchange, Burladingen, Germany). For measurements with OH-tips, the fluid cell was filled with hexadecane (HPLC-grade, Sigma-Aldrich, Darmstadt, Germany). These different setups were chosen

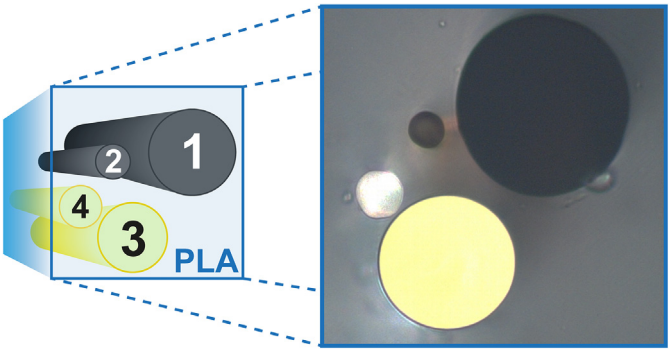

Fig. 1. Spinning dopes were prepared with different compositions, (1) cellulose-lignin, (2) cellulose-xylan-lignin, (3) cellulose, (4) cellulose-xylan, and drawn into fibers with varying diameters. These fibers were embedded in polylactic acid (PLA) and their cross-sections were cut with an ultra-microtome.

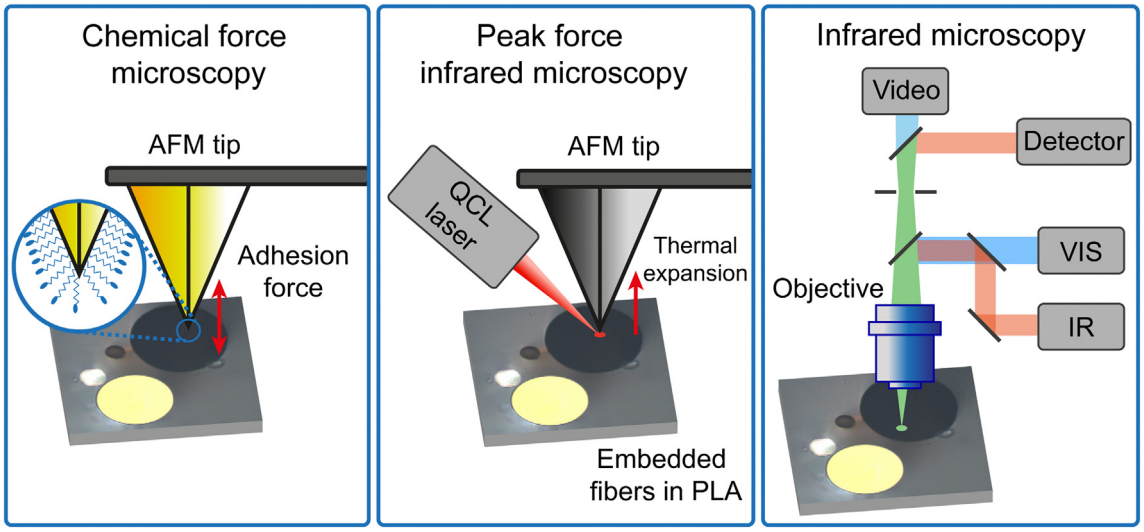

Fig. 2. The ultra-microtomed lignocellulosic substrates were analyzed with three different microscopes to identify surface chemical variations. Adhesive interactions between a functionalized AFM tip and the surface of lignocellulosic fibers showed chemically sensitive images. Peak force infrared microscopy (PFIR) monitored variations in the thermal expansion of the samples induced by a pulsed laser to map spectroscopic contrast. Additional infrared spectra were acquired with far field spatial resolution via infrared microscopy.

since higher adhesion forces have been achieved when the terminating functional groups of the tip are immiscible in the solvent in which the measurements are carried out [23]. Subsequently, a scan area of 45 × 45 μm^2 was chosen so that the cross-section of all four fibers could be scanned in a single image. The measurement parameters were set to a scan speed of 0.1 Hz scanning 128 samples per line. Adhesion forces were derived from PeakForce Quantitative Nanomechanical Mapping (PeakForce QNM™). In that technique, the AFM tip is oscillating at 1 kHz while tapping the sample and scanning the selected scan area. In one peak force cycle, the tip approaches the sample until a predefined set-point and then retracts to its starting position. The maximum force that is needed to break the tip free from the sample when it moves back to the starting position is defined as the adhesion force (Fig. 2), which depends on the chemical character of the surface. In that way, chemically sensitive adhesion maps of the scanned area were generated to visualize surface chemical variation. The AFM probes were calibrated after mapping, i.e. the deflection sensitivity was acquired on a sapphire sample and spring constants were determined by the thermal tune method [24]. The tip radii were acquired on a standard sample (NiO-probe, Science Services GmbH, Munich, Germany) and were between 30 and 35 nm. Adhesion maps and adhesion forces were extracted with an open-source scanning probe microscopy software (Gwyddion, Brno, Czech Republic [25]) and visualized with Origin Pro.

2.5. Peak force infrared microscopy

Peak force infrared microscopy was carried out with an atomic force microscope (MultiMode 8 AFM with Nanoscope *V* controller, Bruker, Santa Barbara, CA, USA). Similarly to CFM described in Section 2.4, peak force tapping was performed at 2 kHz, and the vertical deflection of the AFM cantilever was captured. Additionally, a pulsed quantum cascade laser (QCL, MIRcat, Daylight Photonics, California, USA) was focused between the AFM tip (platinum-coated silicon probe, nominal spring constant 40 N/m, estimated tip radius ~ 25 nm, HQ:NSC15/Pt, MikroMasch, Sofia, Bulgaria) and the surface of the ultra-microtomed sample. Every other peak force cycle, the 100-ns-long laser pulse illuminated the tip-sample contact area, causing photothermal expansion of the microtomed surface and exciting contact resonance of the AFM probe (Fig. 2). If the sample area underneath the tip absorbs the infrared light, photothermal expansion of the microtomed surface occurs. The information on the cantilever deflection containing this response was transferred to a data acquisition card with a sampling rate of 50 MHz. After subtracting the background, i.e., the peak force cycle without laser excitation, the generated PFIR trace was treated with fast-Fourier transform and integrated. This processing resulted in the PFIR signal, which reflects spectroscopic information of the sample [20]. PFIR sensitive images were obtained by setting the laser to a certain wavenumber while scanning an area of 10 × 5 μm^2 of the sample. Point spectra were acquired at a fixed position on the sample by capturing changes in thermal expansion while the laser swept its frequency from 1800 to 900 cm^{-1} in steps of 10 cm^{-1}. Adhesion and stiffness properties were derived using the Derjaguin-Muller-Toporov model [26] from the force-distance curves, in the AFM software when the infrared laser was turned off. The spring constant of the AFM tip was calibrated by the thermal tune method and the deflection sensitivity was determined via the NanoScope software.

2.6. Infrared microscopy

Single point infrared spectra were obtained with a FTIR microscope (Fourier-transform infrared microscope, Hyperion 3000, Bruker Optics, Billerica, MA, USA) in reflectance mode coupled with a spectrometer (VERTEX 70v FT-IR-spectrometer with cooled MCT detector, Bruker). The ultra-microtomed samples were placed on the motorized stage and analyzed with an ATR objective (20× ATR Ge-crystal) with the lowest pressure point setting between sample and crystal during spectra acquisition. The confocal path of the infrared light allows the localization of the spectra (Fig. 2). Measurement parameters were set to a spectral resolution of 2 cm^{-1} covering a spectral range of 4000–650 cm^{-1} and background was recorded between each sample.

3. Results

3.1. Adhesion mapping

Chemical force microscopy measurements revealed varying adhesion forces between functionalized AFM tips and ultra-microtomed regenerated fibers embedded in PLA (Fig. 3). Differentiation between the fibers can be easily made based on the different diameters and colors of the fibers (brown fibers contain lignin), as seen in Fig. 1. In the first setup, adhesion forces of OH-functionalized AFM tips towards

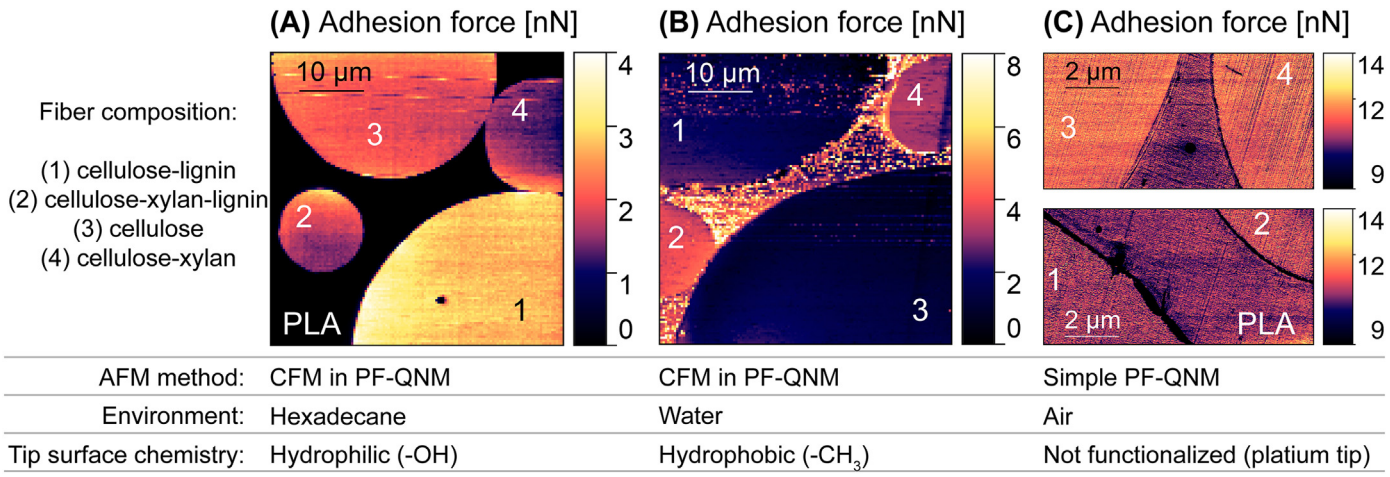

Fig. 3. The spatial distribution of adhesion force between different atomic force microscopy tips and lignocellulosic fibers obtained using chemical force microscopy in liquids or PeakForce Quantitative Nanomechanical measurements in air. The experiments were carried out with varying tip surface functionality (A-C). Corresponding topography images of the ultra-microtomed profiles can be found in Fig. S2 in the supplementary information.

regenerated fibers were analyzed in a hexadecane environment. As seen in Fig. 3A, the hydrophilic tip showed no adhesion forces towards PLA, displayed in black pixels, whereas the lignocellulosic fibers showed adhesion forces up to 4 nN, displayed in bright pixels. The fiber "cellulose-lignin" showed highest magnitudes of adhesion forces with a uniform distribution over its cross-section. Interestingly, the fibers "cellulose-xylan-lignin" and "cellulose-xylan" exhibited gradual transitions and inhomogeneous distributions of adhesion forces with higher magnitudes in specific areas displayed in yellow colour.

In the second setup, interactions towards hydrophobic tips were analyzed in water (Fig. 3B). Here, we observed, that the fibers "cellulose" and "cellulose-lignin" showed low adhesion properties and the three-component fiber "cellulose-xylan-lignin" possessed the strongest affinity towards the CH_3-terminated tip. The highest adhesion forces were acquired on PLA, which exhibited a broad distribution and also had areas of low attractive forces towards the OH-terminated tip. In the third setup, adhesion maps were acquired with non-functionalized platinum tips. These measurements in air depicted overall higher adhesion force towards the platinum-coated tip (Fig. 3C) compared to the measurements in liquids with CH_3- and OH-terminated tips. Additionally, all fibers displayed higher affinities towards the platinum coated tip than to the PLA polymer, whereas the fibers "cellulose" and "cellulose-xylan" both showed slightly higher adhesion forces than the other two fiber types containing lignin.

In Fig. 4, adhesion forces for each fiber type and PLA were extracted by a mask tool and averaged (mask areas can be found in Fig. S1 in the supplementary information). Pt-coated tips exhibited highest magnitudes of adhesion forces (>10 nN), but the differences between the different fiber types were the lowest. However, lignin slightly lowered the affinity of the Pt-coated tip on lignocellulosic surfaces compared to the fibers without lignin. That behavior changes when looking at OH-functionalized tips: the fiber "cellulose-lignin" showed the highest adhesion forces towards the hydrophilic tip compared to the other fiber compositions. Fibers containing xylan, showed low overall adhesion forces towards OH-functionalized tips, but the inhomogeneous adhesion force distribution as seen in Fig. 3A has to be accounted for these fiber types. Contrary to experiments carried out with hydrophilic tips, CH_3-terminated tips showed higher affinities towards fibers containing xylan. Additionally, PLA showed high adhesion towards CH_3-tip modification, but the adhesion forces spread out with high standard deviation (a factor of 4 greater than for fibers), which can be explained by the fact that fibers were closely aligned in that sample, thus, hindering homogenous composition of the PLA embedding matrix between the fibers.

3.2. Spectral imaging

All fibers possessed similar stiffness of approx. 10.4 ± 0.50 GPa (Fig. 5), while PLA showed slightly lower elastic modulus of approx. 10.2 ± 0.2 GPa. Subsequently, the pulsed infrared laser was turned on and focused between the AFM tip apex and the sample while scanning the same area. Tuning the laser to 1026 cm^{-1} enabled detection of areas correlated to C—O stretching [27] and revealed that all fibers showed lower PFIR intensities than PLA at that wavenumber. There is a noticeable gradient within the "cellulose-lignin" fiber with higher PFIR intensities at 1026 cm^{-1} at the edge areas (shell) than in core areas. In contrast, this behavior is not visible in the corresponding stiffness map. In addition, the same area was mapped at 1508 cm^{-1}, indicative of aromatic ring vibrations. In these images, we observed overall low PFIR intensities (<0.1 *V*) with slightly higher intensities of PLA surfaces. Carbonyl groups were detected by setting the laser to a wavenumber of 1723 cm^{-1}. PLA showed the highest PFIR intensities in that setup,

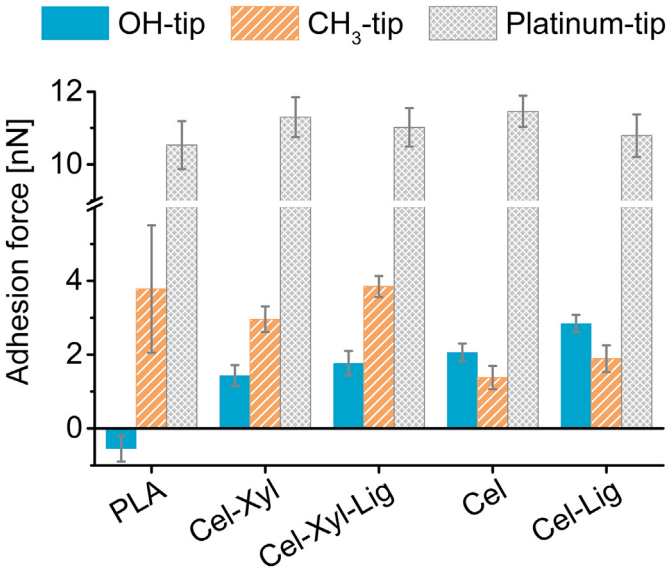

Fig. 4. Average adhesion forces (error bars show standard deviation) between different tips and regenerated fibers (Cel…cellulose, Xyl…xylan, Lig…lignin) and matrix polymer (PLA…polylactic acid).

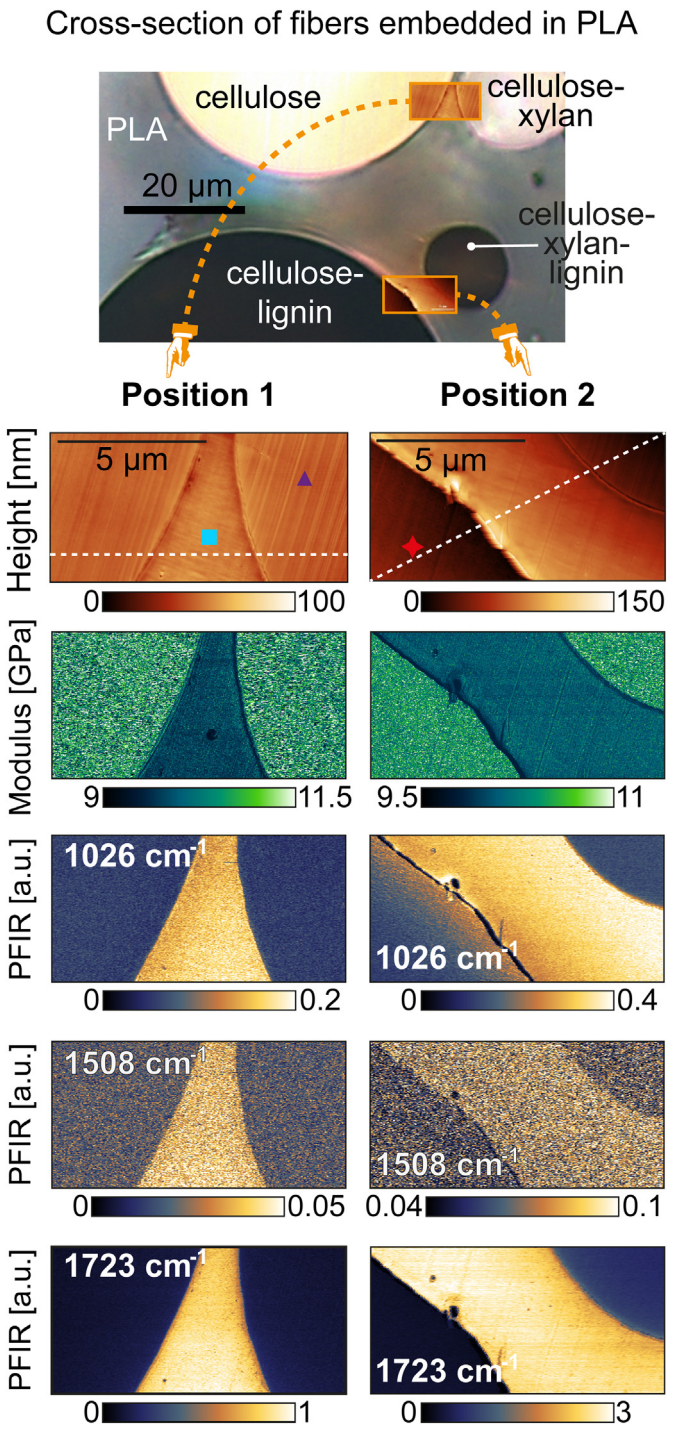

Fig. 5. PFIR imaging revealed the topography, Young's modulus, and PFIR maps at certain wavenumbers of the same selected lignocellulosic fibers cross-sections. Dashed white lines in the height images show the position of extracted line profiles in Fig. 6; symbols show the position of the collected point spectra in Fig. 7.

followed by the three-component "cellulose-xylan-lignin" fiber. The resolution of the chemical mapping was found to be 20 nm based on the applied scanning settings (512 px × 256 px).

Cross-profiles were extracted from the PFIR maps (Fig. 6) to identify gradients in the PFIR data, which would indicate different distributions of the fiber components in the cross-section. Within these maps, higher PFIR intensities were observed in thin shell areas in the "cellulose" and "cellulose-xylan" fibers with a width of about 1.3 µm marked by red

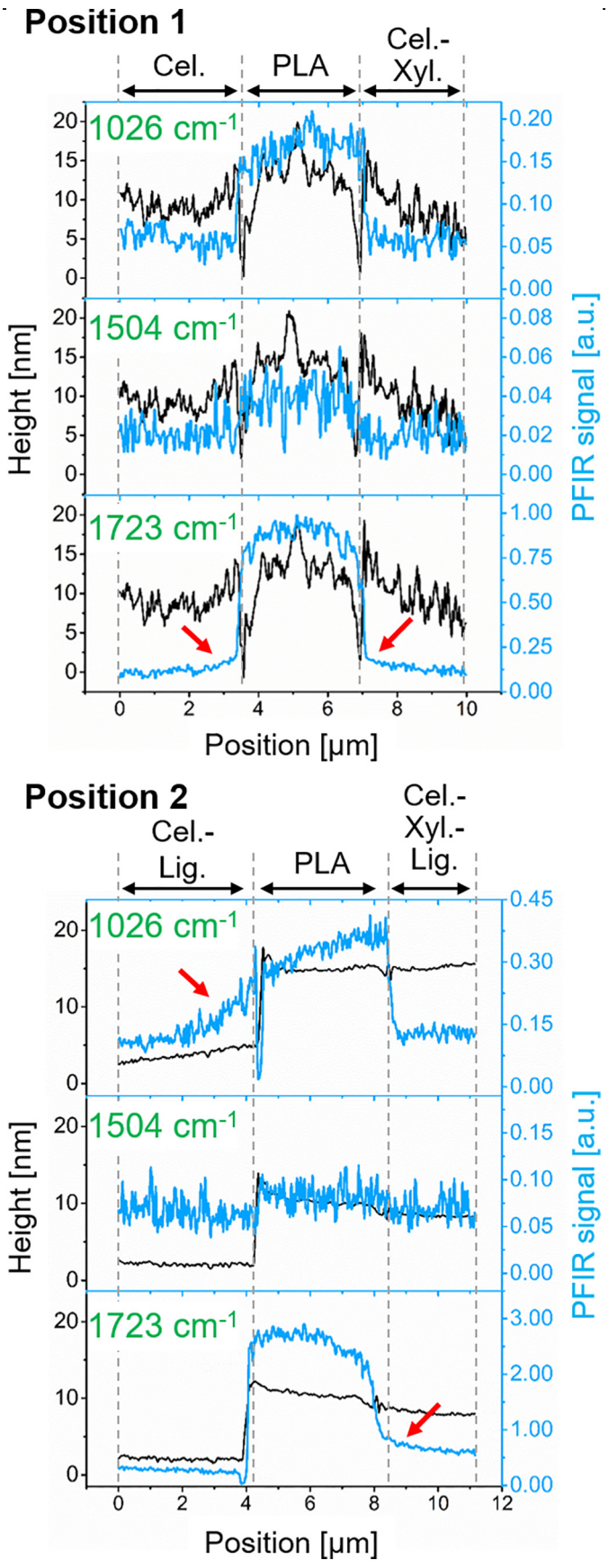

Fig. 6. Line profiles were extracted from PFIR maps at 1026 cm^{-1}, 1508 cm^{-1} and 1723 cm^{-1} with their corresponding height profiles. Signal changes towards certain edge areas are marked with red arrows (Cel…cellulose, Xyl…xylan, Lig…lignin). The profiles were extracted from the same area indicated with white dashed lines in height images in Fig. 5.

arrows in Fig. 6. The "cellulose-xylan-lignin" fiber showed slightly higher PFIR intensities at 1723 cm^{-1} than the "cellulose-lignin" fiber. A shell area of about 3 μm thickness having higher PFIR intensities than the core of the fiber can be seen at 1026 cm^{-1} in the "cellulose-lignin" fiber at position 2. The core-shell behavior was not apparent in the line profiles when the laser was tuned to 1508 cm^{-1}, but the PFIR point spectra revealed a poorly defined peak at this wavenumber for both fibers and PLA matrix.

IR point spectra were taken at fixed positions in regenerated fibers and PLA matrix by PFIR and compared to conventional ATR-FTIR and infrared microscopy spectra. Infrared microscopy offers the possibility to collect IR spectra at the fibers cross-section, which analyzes the sample in the same molecular orientation and structural condition as in PFIR spectra. The locations where the infrared microscopy spectra were acquired can be seen in Fig. S3 in the supplementary information. In Fig. 7, the peaks in the spectrum of PLA were assigned to C═O vibration at 1746 cm^{-1}, –C-H bending vibration at 1452 cm^{-1}, and -C–O vibration at 1180 cm^{-1} and 1082 cm^{-1} [27–30]. Cellulose peaks in the spectrum of the "cellulose-xylan" and "cellulose-lignin" fibers were assigned to –OH bending of water in cellulose structures at 1635 cm^{-1}, –OH in plane bending at 1336 cm^{-1}, C–O–C asymmetric stretching at 1158 cm^{-1} and C—O stretching 1026 cm^{-1} [31,32]. The presence of lignin was detected in the "cellulose-lignin" fiber by a peak at 1504 cm^{-1} that is assigned to asymmetric ring stretching [33]. When comparing the FTIR spectra of the "cellulose" and "cellulose-xylan" fibers, the addition of xylan showed no considerable changes in the IR spectra (Fig. S4 in the supplementary information).

4. Discussion

The applied microscopy techniques showed the surface chemical properties of Ioncell-F fibers. Adhesion properties tested with CFM confirmed the high adhesion contrasts between PLA and pure cellulose fibers obtained with either hydrophilic tips in non-polar medium or hydrophobic tips in water (Fig. 3). The distinct affinity of the PLA matrix and cellulose-derived fibers for hydrogen-binding and non-polar moieties pointed to potentially strong incompatibility between the two components. Addition of lignin did not change this relation substantially. However, the incorporation of xylan showed beneficial effects indicating reduced differences in polarity between PLA and regenerated cellulose fibers, thus, potentially leading to their improved compatibility in composite materials. These results are consistent with previous findings where pure cellulose surfaces displayed the lowest adhesion forces towards PLA probes in water in comparison to cellulose-hemicellulose surfaces [11,34] presenting lower polarity interface compared to cellulose.

The strong influence of capillary forces at the cellulosic surfaces, apparent in the CFM experiments performed with platinum tips in air, could be eliminated by performing the CFM experiments in a specific liquid environment to target high adhesion contrast between the chemically functionalized AFM tips and the Ioncell-F fibers. Especially when the microtomed surfaces were analyzed with hydrophilic tips, we could see a non-uniform distribution of adhesion within the fibers contained xylan (Fig. 3A). These results are in line with the finding that the surfaces of the Lyocell fibers are enriched with xylan as demonstrated by compositional polysaccharide analysis (high-performance capillary zone electrophoresis) of the outer surface of enzymatically degraded cellulosic fibers [13]. This previous study reveals that a thin hemicellulose-rich outermost layer exists – we could not observe a clear layer with CFM, but from the observed adhesion gradients at the "cellulose-xylan-lignin" and "cellulose-xylan" fibers we assume a higher concentration of xylan in certain regions. One explanation for the enrichment phenomena could be the higher diffusion rate of short chain molecules, i.e. xylan or lignin, during coagulation in the cellulose fiber regeneration process. It is supposed that the first event of regeneration from [DBNH]OAc solution is induced by spinodal decomposition [35], which could lead to an inhomogeneous distribution of the fiber components.

Contrary to CFM, in which the adhesion force serves as the indirect key parameter to track surface chemical variation, PFIR identifies changes in the thermal expansion of the sample that can be translated into the spectroscopic signature of distinct organic functional groups (Table 1). The spectroscopic maps acquired with PFIR show slight gradients within fibers containing xylan, but interestingly, the strongest gradient was found within the "cellulose-lignin" fiber (Fig. 6). Several reasons could explain such behavior. First, residual xylan of 4.35 wt% was found in this fiber [10], which might be enriched at the core of that fiber. Second, lignin deposition on the fiber surface was found in the fiber spinning bath [36], which could also explain a gradient within the fiber cross-section. Third, a clear skin-core structure might have been developed, as seen in the case of standard viscose fibers with a thickness of 2 μm due to orientation differences [12]. There is also

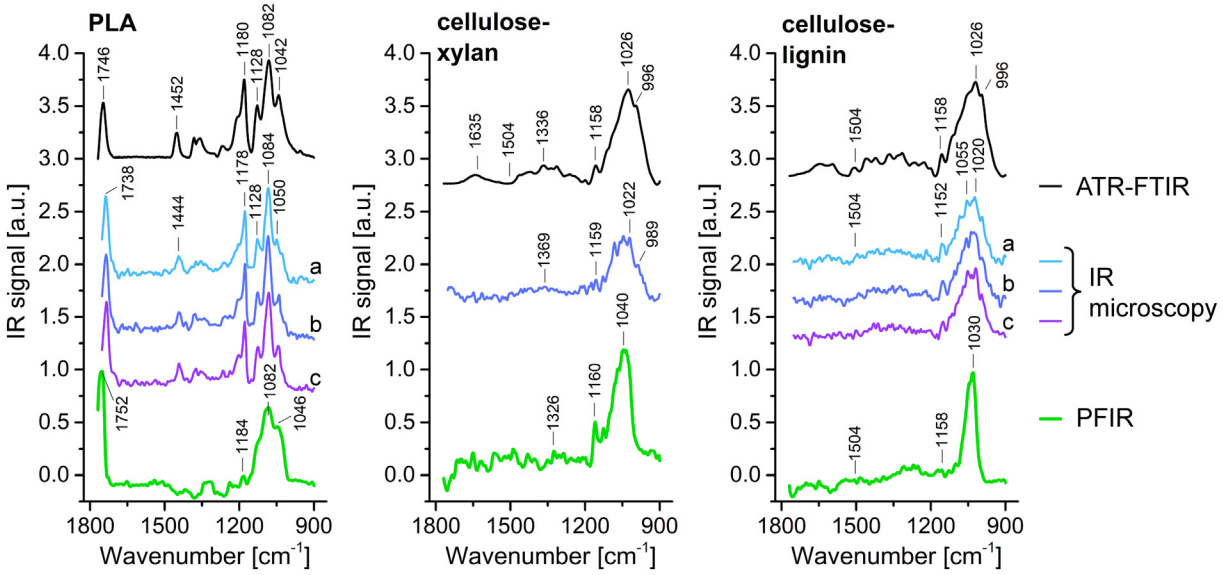

Fig. 7. Conventional ATR-FTIR spectra, IR microscopy spectra, and PFIR point spectra were collected at each lignocellulosic fiber and PLA. The spectra were normalized at 1026 cm^{-1} (offset for clarity). The positions of PFIR spectra are marked with symbols on height images in Fig. 5. The different blue colors in IR microscopy set refer to the different sample positions for the acquisition of the spectra. The different positions of IR microscopy spectra (a-c) can be found in Fig. S3 in the supplementary data.

Table 1
Comparison of the microscopic techniques applied to characterization of regenerated cellulose fibers.

	Chemical force microscopy	Peak force infrared microscopy	Infrared microscopy
Detected signal	Adhesion force between AFM tip and sample	Photothermal expansion of sample translated from AFM tip deflection	Light absorbance of characteristic molecule vibrations
Information output	-Topography -Mechanical maps (adhesion and stiffness)	-IR maps -Point IR spectra -Topography -Mechanical maps	-Spectral maps -Point spectra
Lateral resolution	~ 30 nm (depending on condition and modification of tip)	Below 20 nm	Depending on light wavelength and objective
Requirements	-Smooth surface -Preferable liquid environment	Smooth surface	Even surface
Challenges	-Tip preparation -Tip artefacts and contamination -Sample swelling	-Complex setup; not yet commercially available -Tip artefacts, and contamination	-Requires physical contact -Compression of sample by ATR crystal

evidence that Lyocell fibers possess a very thin skin of 100 nm in dry state [14]. These structural changes were not detected in our performed topography or stiffness maps; thus, the chemical composition is more likely to influence the PFIR signal. The elastic modulus of 10.4 GPa was uniformly distributed in all fibers and independent of the different draw ratios, in contrast to previous studies in which the elastic modulus increases from approx. 12.5 GPa at a draw ratio of 1 to 17 GPa at a draw ratios of 7 [2]. The differences with respect to the effect of the draw ratio and the magnitude of the modulus might be based on the differences in the testing methods – tensile testing on the macroscale and PFIR/PF-QNM mapping on the nanoscale – and different storage times between fiber production and testing.

Overall, Ioncell-F fibers showed lower PFIR intensities than PLA (Fig. 5), supposedly, reflecting the differences in the volume number density of the corresponding functional groups. Another factor that could influence observed contrast for regenerated fibers is the mutual alignment between laser polarization and oriented elements in these fibers. It was shown that cellulose chains are highly oriented and run parallel to the longitudinal axis of Ioncell-F fibers and that the molecules are packed closely [1]. In a recent study, the inner structure of Ioncell-F fibers has been examined, and the influence of three different structural domains was reported: oriented cellulose crystallites, amorphous regions, that align along the chain axes, and elongated oriented voids [2]. Since the fibers were cut perpendicular to the fiber axis in the current study, the preferred molecular orientation is preserved, and its role can be evaluated with polarization dependent studies.

The characterization methods applied in this paper are compared in Table 1. The benefits of CFM and PFIR are the absence of a strong undesirable background, such as auto-fluorescence that influences the measurements with Raman microscopy or strong capillary forces that influence measurements with unmodified tips in ambient air, and that neither staining nor thin-sectioning is needed, thus, greatly simplifying sample preparation. The PFIR microscopy stands out as the tool having high spatial resolution and delivering real spectroscopic information together with mechanical mapping. For CFM, the proper choice of the tip functionalization and the liquid medium for imaging allows adapting the setup to the specifics of the analyzed cellulose fiber samples. Here, the capillary forces on hygroscopic cellulosic materials unavoidable in PFIR imaging could be eliminated by performing the CFM experiments under liquids. Spectra obtained from infrared microscopy were found to be supportive of the PFIR results. The limitations of the CFM and PFIR arise from the general challenges in the AFM based techniques: the use of specialized tip preparation (chemical modification or metal coating) and caution needed to be taken regarding tip contamination and wear.

5. Conclusion

We demonstrated that chemical force microscopy and peak force infrared microscopy are effective techniques to visualize surface chemical variation of micro-profiles of regenerated biobased fibers. Both approaches revealed gradients within certain fibers, even though the detected signals to trace chemical changes are different in the two microscopy setups. CFM revealed varying adhesion forces between functionalized AFM tips and differently tuned Ioncell-F fibers. PFIR traced changes of thermal expansion induced by a pulsed infrared laser. Both methods suggested that xylan plays an important role in influencing the distribution of adhesion forces and IR intensities across fiber-matrix interface. Therefore, we conclude that adhesion forces are dependent on the chemical composition of lignocellulosic fiber and that the cross-section of Ioncell-F fibers shows a heterogeneous distribution of surface chemical characteristics at certain fiber compositions. The methods applied in this work could probe quantitatively surface chemical properties and, thus, represent a rigorous approach to visualize these properties with the nanoscopic spatial resolution in order to optimize the embedding process of lignocellulosic fibers inside a composite material.

CRediT authorship contribution statement

Claudia Gusenbauer: Conceptualization, Investigation, Writing - original draft, Visualization. **Tiina Nypelö:** Investigation. **Devon S. Jakob:** Investigation, Writing - review & editing. **Xiaoji G. Xu:** Resources, Methodology, Writing - review & editing, Supervision. **Dmitri V. Vezenov:** Writing - review & editing, Supervision. **Shirin Asaadi:** Resources, Writing - review & editing. **Herbert Sixta:** Resources, Writing - review & editing. **Johannes Konnerth:** Conceptualization, Project administration, Funding acquisition, Supervision.

Declaration of competing interest

The authors declare no competing interests.

Acknowledgment

This work is funded by the Austrian Science Fund FWF [project number: I 2247], the Lower Austrian Research and Education Society NFB [project number: SC16-004], the Swiss National Science Foundation SNSF [project number: 160041] and the Austrian Marshall Plan Foundation. Furthermore, we thank Jérôme Colson for supporting the CFM experiments. We thank Chalmers Materials Analysis Laboratory and Dr. Katarina Logg for access and support with IR microscopy.

Appendix A. Supplementary data

Supplementary data to this article can be found online at https://doi.org/10.1016/j.ijbiomac.2020.10.145.

References

[1] A. Michud, M. Tanttu, S. Asaadi, Y. Ma, E. Netti, P. Kääriainen, A. Persson, A. Berntsson, M. Hummel, H. Sixta, Ioncell-F: ionic liquid-based cellulosic textile fibers as an alternative to viscose and Lyocell, Text. Res. J. 86 (5) (2016) 543–552.
[2] S. Asaadi, M. Hummel, P. Ahvenainen, M. Gubitosi, U. Olsson, H. Sixta, Structural analysis of Ioncell-F fibres from birch wood, Carbohydr. Polym. 181 (2018) 893–901.
[3] H. Sixta, A. Michud, L. Hauru, S. Asaadi, Y. Ma, A.W. King, I. Kilpeläinen, M. Hummel, Ioncell-F: a high-strength regenerated cellulose fibre, Nordic Pulp & Paper Research Journal 30 (1) (2015) 43–57.
[4] A. Parviainen, R. Wahlström, U. Liimatainen, T. Liitiä, S. Rovio, J.K.J. Helminen, U. Hyväkkö, A.W.T. King, A. Suurnäkki, I. Kilpeläinen, Sustainability of cellulose dissolution and regeneration in 1,5-diazabicyclo[4.3.0]non-5-enium acetate: a batch simulation of the IONCELL-F process, RSC Adv. 5 (85) (2015) 69728–69737.
[5] M.J. John, S. Thomas, Biofibres and biocomposites, Carbohydr. Polym. 71 (3) (2008) 343–364.
[6] N. Graupner, A.S. Herrmann, J. Müssig, Natural and man-made cellulose fibre-reinforced poly(lactic acid) (PLA) composites: an overview about mechanical characteristics and application areas, Compos. A: Appl. Sci. Manuf. 40 (6) (2009) 810–821.
[7] M. Shibata, S. Oyamada, S.-i. Kobayashi, D. Yaginuma, Mechanical properties and biodegradability of green composites based on biodegradable polyesters and lyocell fabric, J. Appl. Polym. Sci. 92 (6) (2004) 3857–3863.
[8] N. Graupner, H. Fischer, G. Ziegmann, J. Müssig, Improvement and analysis of fibre/matrix adhesion of regenerated cellulose fibre reinforced PP-, MAPP- and PLA-composites by the use of Eucalyptus globulus lignin, Compos. Part B 66 (2014) 117–125.
[9] S.C. Singh, Z.V.P. Murthy, Study of cellulosic fibres morphological features and their modifications using hemicelluloses, Cellulose 24 (8) (2017) 3119–3130.
[10] T. Nypelö, S. Asaadi, G. Kneidinger, H. Sixta, J. Konnerth, Conversion of wood-biopolymers into macrofibers with tunable surface energy via dry-jet wet-spinning, Cellulose 25 (9) (2018) 5297–5307.
[11] J. Colson, T. Pettersson, S. Asaadi, H. Sixta, T. Nypelö, A. Mautner, J. Konnerth, Adhesion properties of regenerated lignocellulosic fibres towards poly (lactic acid) microspheres assessed by colloidal probe technique, J. Colloid Interface Sci. 532 (2018) 819.
[12] M. Müller, C. Riekel, R. Vuong, H. Chanzy, Skin/core micro-structure in viscose rayon fibres analysed by X-ray microbeam and electron diffraction mapping, Polymer 41 (7) (2000) 2627–2632.
[13] J. Sjöberg, A. Potthast, T. Rosenau, P. Kosma, H. Sixta, Cross-sectional analysis of the polysaccharide composition in cellulosic fiber materials by enzymatic peeling/high-performance capillary zone electrophoresis, Biomacromolecules 6 (6) (2005) 3146–3151.
[14] K.C. Schuster, P. Aldred, M. Villa, M. Baron, R. Loidl, O. Biganska, S. Patlazhan, P. Navard, H. Rüf, E. Jericha, Characterising the emerging lyocell fibres structures by ultra small angle neutron scattering (USANS), Lenzinger Berichte 82 (2003) 107–117.
[15] C.D. Frisbie, L.F. Rozsnyai, A. Noy, M.S. Wrighton, C.M. Lieber, Functional group imaging by chemical force microscopy, Science 265 (5181) (1994) 2071.
[16] J.C. Bastidas, R. Venditti, J. Pawlak, R. Gilbert, S. Zauscher, J.F. Kadla, Chemical force microscopy of cellulosic fibers, Carbohydr. Polym. 62 (4) (2005) 369.
[17] C. Gusenbauer, E. Cabane, N. Gierlinger, J. Colson, J. Konnerth, Visualization of the stimuli-responsive surface behavior of functionalized wood material by chemical force microscopy, Sci. Rep. 9 (1) (2019), 18569, .
[18] B. Arslan, X. Ju, X. Zhang, N.I. Abu-Lail, Heterogeneity and specificity of nanoscale adhesion forces measured between self-assembled monolayers and lignocellulosic substrates: a chemical force microscopy study, Langmuir 31 (37) (2015) 10233–10245.
[19] D. Yan, K. Li, Evaluation of inter-fiber bonding in wood pulp fibers by chemical force microscopy, Journal of Materials Science Research 2 (1) (2013) 23.
[20] L. Wang, H. Wang, M. Wagner, Y. Yan, D.S. Jakob, X.G. Xu, Nanoscale simultaneous chemical and mechanical imaging via peak force infrared microscopy, Sci. Adv. 3 (6) (2017).
[21] W. Li, H. Wang, X.G. Xu, Y. Yu, Simultaneous nanoscale imaging of chemical and architectural heterogeneity on yeast cell wall particles, Langmuir 36 (2020) 6169–6177.
[22] D.S. Jakob, L. Wang, H. Wang, X.G. Xu, Spectro-mechanical characterizations of kerogen heterogeneity and mechanical properties of source rocks at 6 nm spatial resolution, Anal. Chem. 91 (14) (2019) 8883–8890.
[23] A. Noy, D.V. Vezenov, C.M. Lieber, Chemical force microscopy nanoscale probing of fundamental chemical interactions, in: A. Noy (Ed.), Handbook of Molecular Force Spectroscopy, Springer, Boston, MA 2008, pp. 97–122.
[24] J.L. Hutter, J. Bechhoefer, Calibration of atomic-force microscope tips, Rev. Sci. Instrum. 64 (7) (1993) 1868–1873.
[25] D. Nečas, P. Klapetek, Gwyddion: An Open-Source Software for SPM Data Analysis, vol. 10, 2012 181 (1).
[26] B. Derjaguin, V. Muller, Y. Toporov, On different approaches to the contact mechanics, JCIS (1980) 293–294.
[27] M. Hesse, H. Meier, B. Zeeh, Spektroskopische Methoden in der organischen Chemie, Georg Thieme Verlag, Stuttgart, New York, 2005.
[28] K. Shameli, M.B. Ahmad, W.M.Z.W. Yunus, N.A. Ibrahim, R.A. Rahman, M. Jokar, M. Darroudi, Silver/poly (lactic acid) nanocomposites: preparation, characterization, and antibacterial activity, Int. J. Nanomedicine 5 (2010) 573.
[29] S.-l. Yang, Z.-H. Wu, W. Yang, M.-B. Yang, Thermal and mechanical properties of chemical crosslinked polylactide (PLA), Polym. Test. 27 (8) (2008) 957–963.
[30] M.G. Rimoli, L. Avallone, P. de Caprariis, A. Galeone, F. Forni, M.A. Vandelli, Synthesis and characterisation of poly(d,l-lactic acid)–idoxuridine conjugate, J. Control. Release 58 (1) (1999) 61–68.
[31] F. Carrillo, X. Colom, J.J. Suñol, J. Saurina, Structural FTIR analysis and thermal characterisation of lyocell and viscose-type fibres, Eur. Polym. J. 40 (9) (2004) 2229–2234.
[32] M.L. Nelson, R.T. O'Connor, Relation of certain infrared bands to cellulose crystallinity and crystal latticed type. Part I. Spectra of lattice types I, II, III and of amorphous cellulose, J. Appl. Polym. Sci. 8 (3) (1964) 1311–1324.
[33] N.M. Stark, D.J. Yelle, U.P. Agarwal, Techniques for characterizing lignin, Lignin in polymer composites (2016) 49–66.
[34] G. Raj, E. Balnois, M.-A. Helias, C. Baley, Y. Grohens, Measuring adhesion forces between model polysaccharide films and PLA bead to mimic molecular interactions in flax/PLA biocomposite, J. Mater. Sci. 47 (5) (2012) 2175–2181.
[35] Y. Nishiyama, S. Asaadi, P. Ahvenainen, H. Sixta, Water-induced crystallization and nano-scale spinodal decomposition of cellulose in NMMO and ionic liquid dope, Cellulose 26 (1) (2019) 281–289.
[36] Y. Ma, S. Asaadi, L.-S. Johansson, P. Ahvenainen, M. Reza, M. Alekhina, L. Rautkari, A. Michud, L. Hauru, M. Hummel, H. Sixta, High-strength composite fibers from cellulose–lignin blends regenerated from ionic liquid solution, ChemSusChem 8 (23) (2015) 4030–4039.